Direct Observation of Asymmetric $^{1}H/^{14}N$ Triplets and Applications of Asymmetric Dipole−Dipole Splittings to Structure Determination by Solid-State NMR Spectroscopy

R. McNamara, C. H. Wu, L. E. Chirlian, and S. J. Opella*

Contribution from the Department of Chemistry, University of Pennsylvania, Philadelphia, Pennsylvania 19104

Received March 16, 1995[⊗]

Abstract: High-resolution solid-state NMR spectra of ^{1}H nuclei directly bonded to ^{14}N nuclei can be extracted from two-dimensional $^{1}H/^{14}N$ heteronuclear correlation spectra of single crystal samples. The ^{1}H resonances are asymmetric triplets, since the heteronuclear dipole−dipole interaction between a spin one-half ^{1}H and a spin one ^{14}N is influenced by the large ^{14}N quadrupole coupling constant and can be observed in both ^{14}N fundamental ($\Delta m = 1$) and ^{14}N overtone ($\Delta m = 2$) spectra. ^{14}N fundamental spectra have two resonances for each magnetically distinct ^{14}N nucleus, each of which is a doublet in the heteronuclear correlation spectra; the asymmetric ^{1}H triplets can be reconstructed from the doublets of both resonances. ^{14}N overtone spectra are simpler, since they have a single asymmetric ^{1}H triplet associated with a single ^{14}N resonance for each magnetically distinct ^{14}N nucleus. ^{1}H chemical shift frequencies, the splittings from $^{1}H/^{14}N$ heteronuclear dipole−dipole couplings, ^{14}N quadrupole splittings, and ^{14}N second-order shifts can all be measured with both fundamental and overtone $^{1}H/^{14}N$ heteronuclear correlation spectra. In addition, the ^{1}H and ^{14}N resonance frequencies for the bonded hydrogen and nitrogen nuclei are correlated in these spectra. The spectral parameters from asymmetric $^{1}H/^{14}N$ triplets are demonstrated to offer substantial advantages over those of the corresponding symmetric $^{14}N/^{1}H$ doublets for determining structures of peptides by solid-state NMR spectroscopy, even though both sets of parameters arise from the same dipole−dipole interactions.

Introduction

The dipole−dipole interaction between two nuclei is a valuable source of structural information in solid-state NMR spectroscopy because it provides directly measurable spectral parameters that are readily interpretable in terms of distances and angles. The dipole−dipole interaction between two spin one-half nuclei results in each of their resonances being split into a symmetric doublet. The magnitude of the splitting is a function of the distance between the two nuclei, the angle between the internuclear vector and the direction of the applied magnetic field, and a few physical constants for both homonuclear and heteronuclear dipole−dipole interactions.[1] A wide variety of experimental methods have been used to observe the symmetric spectral manifestations of dipole−dipole interactions between two spin one-half nuclei as resolved splittings in single crystal[2−4] and oriented samples,[5] well-defined Pake powder patterns,[2,4,6,7] broad lines characterized by second moments[8] in stationary unoriented samples, and sidebands in unoriented[9] and oriented[10] samples spinning at the magic angle. In many applications multidimensional spectra are required to segregate the spectral parameters due to the dipole−dipole interactions of interest from those of other spin interactions.

The simplicity of experimental and theoretical aspects of the dipole−dipole interaction between two different spin one-half nuclei contributes to its popularity and reliability in structure determination. The dipole−dipole interaction between a spin one-half nucleus and a spin one (or greater) nucleus is also of interest—not only because chemical groups containing these nuclei are present in most molecules, but also because much more spectroscopic and structural information is available than in the case of interactions between two spin one-half nuclei. However, the considerable complexity that accompanies the presence of a large quadrupole coupling constant in a spin one (or greater) nucleus results in a substantial loss of elegance in the analysis compared to that for two spin one-half nuclei. This complexity is the reason that one of the seminal papers in the field of solid-state NMR spectroscopy describes how to take the quadrupole interaction into account in the derivation of internuclear distances from dipole−dipole interactions.[11] This initial report was concerned with the second moments of ^{1}H nuclei interacting with spin seven-halves metal nuclei with large quadrupole coupling constants in stationary powder samples. Much of the subsequent work has focused on the influence of ^{14}N on ^{13}C resonances in single crystals[12−17] and in powder

[⊗] Abstract published in *Advance ACS Abstracts*, July 1, 1995.

(1) Abragam, A. *The Principles of Nuclear Magnetism*; Oxford University Press: Oxford, UK, 1961.
(2) Pake, G. E. *J. Chem. Phys.* **1948**, *16*, 327−336.
(3) Hester, R. K.; Ackerman, J. L.; Neff, B. L.; Waugh, J. S. *Phys. Rev. Lett.* **1976**, *36*, 1081−1083.
(4) Wu, C. H.; Ramamoorthy, A.; Opella, S. J. *J. Magn. Reson.* **1994**, *A109*, 265−269.
(5) Opella, S. J.; Waugh, J. S. *J. Chem. Phys.* **1977**, *66*, 4919−4924.
(6) Linder, M.; Hohener, A.; Ernst, R. R. *J. Chem. Phys.* **1980**, *73*, 4959−4970.
(7) Ramamoorthy, A.; Wu, C. H.; Opella, S. J. *J. Magn. Reson.* **1995**, *B107*, 88−90.
(8) Van Vleck, J. H. *Phys. Rev.* **1948**, *74*, 1168−1183.
(9) Munowitz, M. G.; Griffin, R. G.; Bodenhausen, G.; Huang, T. H. *J. Am. Chem. Soc.* **1981**, *103*, 2529−2533.
(10) Bluemich, B.; Boeffel, C.; Harbison, G. S.; Yang, Y.; Spiess, H. W. *Ber. Bunsen-Ges. Phys. Chem.* **1987**, *91*, 1100−1103.
(11) VanderHart, D. L.; Gutowsky, H. S.; Farrar, T. C. *J. Am. Chem. Soc.* **1967**, *89*, 5056−5057.
(12) Naito, A.; Ganapathy, S.; Akasaka, K.; McDowell, C. A. *J. Chem. Phys.* **1983**, *74*, 3190−3197.
(13) Naito, A.; Ganapathy, S.; Raghunathan, P.; McDowell, C. A. *J. Chem. Phys.* **1983**, *79*, 4173−4182.
(14) McDowell, C. A.; Naito, A.; Sastry, D. L.; Takegoshi, K. *J. Magn. Reson.* **1986**, *69*, 283−292.
(15) Alla, M.; Kundla, E.; Lippmaa, E. *JETP Lett.* **1978**, *27*, 208−211.
(16) Ramanathan, K. V.; Opella, S. J. *J. Magn. Reson.* **1988**, *78*, 367−370.

0002-7863/95/1517-7805$09.00/0

samples spinning at the magic angle.[18-33] Although several other cases have been examined,[34,35] relatively little attention has been paid to ^1H nuclei bonded to ^{14}N[36-38] or other nuclei with spin one (or greater); this undoubtedly reflects the difficulties inherent in obtaining experimental high-resolution spectra of ^1H nuclei bonded to nuclei with substantial quadrupole coupling constants.

The dipole−dipole interaction between a spin one-half and a spin one nucleus is described with the energy level diagram in Figure 1 and the corresponding simulated spectra in Figure 2. Section A in both figures shows the effect of the Zeeman interaction between the applied magnetic field and the spin one-half nucleus, where transitions between the two energy levels give a single line spectrum with the precise resonance frequency determined by other nuclear spin interactions such as the chemical shift. Section B in Figure 1 illustrates that the dipole−dipole interaction between a spin one nucleus and a spin one-half nucleus splits each of the Zeeman levels of the spin one-half nucleus into three equally spaced levels. The corresponding spectrum of the spin one-half nucleus is a symmetric triplet, as shown in part B of Figure 2, when the quadrupole coupling constant of the spin one nucleus is much smaller than the Larmor frequency. A large quadrupole interaction interferes with the polarization of the spin one nucleus along the direction of the applied magnetic field sufficiently to alter the dipole−dipole interaction. This is illustrated in section C of Figure 1 by the shifting of all three energy levels of the spin one nucleus, which results in an asymmetric triplet spectrum of the spin one-half nucleus, as shown in Figure 2C. The large 3−4 MHz coupling

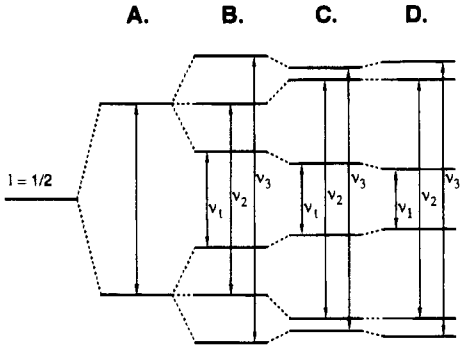

Figure 1. Energy level diagram for a spin $I = {}^1/_2$ nucleus interacting with an external magnetic field and a nearby spin $S = 1$ nucleus. Differences in energy values are expressed as vertical displacements (not to scale) of lines relative to the zero-energy level indicated by the solid line on the left labeled $I = {}^1/_2$. The various effects are shown separately and are designated with capital letters on the top of the diagram. (A) The external magnetic results in two energy levels for an isolated spin $I = {}^1/_2$ nucleus. (B) The dipole−dipole interaction between a spin $I = {}^1/_2$ nucleus and a nearby spin $S = 1$ nucleus splits each of the spin $I = {}^1/_2$ levels into three energy levels. (C) The energy levels from the dipole−dipole interaction are perturbed by the presence of the quadrupole interaction in the spin $S = 1$ nucleus. (D) There are second-order effects on the energy levels when the nuclear quadrupole coupling constant is large compared to the applied magnetic field. A second-order shift lowers the lowest energy level and raises the highest energy level and the middle level is unaffected.

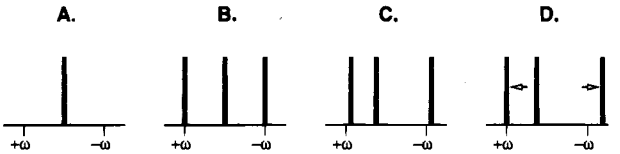

Figure 2. Schematic "stick" spectra that illustrate the spectral manifestations of transitions between the energy levels of a spin $I = {}^1/_2$ nucleus interacting with an external magnetic field and a nearby spin $S = 1$ nucleus as depicted in Figure 1. The same capital letter designations are used for the corresponding energy level diagrams (Figure 1) and "stick" spectra (Figure 2). (A) An isolated spin $I = {}^1/_2$ nucleus gives a single line spectrum in the presence of an external magnetic field. (B) A spin $I = {}^1/_2$ nucleus dipole−dipole coupled to a spin $S = 1$ nucleus with a small quadrupole coupling constant gives a symmetric triplet spectrum. (C) A spin $I = {}^1/_2$ nucleus dipole−dipole coupled to a spin $S = 1$ nucleus with a large quadrupole coupling constant gives an asymmetric triplet spectrum. (D) The second-order quadrupole effect increases the splitting of the two outer lines (arrows) of the asymmetric triplet shown in part C.

constant of an amide nitrogen[39,40] causes substantial spectral perturbations through this mechanism, since fundamental ^{14}N resonance frequencies are in the range of 10−100 MHz on currently available spectrometers.

Second-order effects perturb energy levels (Figure 1D) and splittings (Figure 2D) when the spin one nucleus has a large quadrupole coupling constant. A second-order effect is crucial for ^{14}N overtone experiments because it makes the transition between the lowest and highest energy levels of the spin one nitrogen nucleus partially allowed. As a result, the $\Delta m = 2$ ^{14}N overtone transitions can be excited and detected experimentally.[41-43] ^{14}N overtone NMR spectra consist of a single line resonance, near twice the Larmor frequency, for each unique

(17) Ramanathan, K. V.; Opella, S. J. In *NMR and X-ray Crystallography: Interfaces and Challenges*; Ettes, M. C., Ed. *Trans ACA (AID, NY)* **1989**, *24*, 145−153.
(18) Lippmaa, E.; Alla, M.; Raude, H.; Teeaar, R.; Heinmaa, I.; Kundla, E. *Proceedings of the 20th Congress Ampere, Tallinn*; Springer: Berlin, 1979; p 87.
(19) Kundla, E.; Alla, M. *Proceedings of the 20th Congress Ampere, Tallinn*; Springer: Berlin, 1979; p 92.
(20) Opella, S. J.; Frey, M. H.; Cross, T. A. *J. Am. Chem. Soc.* **1979**, *101*, 5856−5857.
(21) Groombridge, C. J.; Harris, R. K.; Packer, K. J.; Say, B. J.; Tanner, S. F. *J. Chem. Soc., Chem. Commun.* **1980**, *4*, 174−175.
(22) Balimann, G. E.; Groombridge, C. J.; Harris, R. K.; Packer, K. J.; Say, B. J.; Tanner, S. F. *Philos. Trans. R. Soc. London Ser. A* **1981**, *299*, 643−663.
(23) Hexem, J. G.; Frey, M. H.; Opella, S. J. *J. Am. Chem. Soc.* **1981**, *103*, 224−226.
(24) Opella, S. J.; Hexem, J. G.; Frey, M. H.; Cross, T. A. *Philos. Trans. R. Soc. London Ser. A* **1981**, *299*, 665−683.
(25) Zumbulyadis, N.; Henrichs, P. M.; Young, R. H. *J. Chem. Phys.* **1981**, *75*, 1603−1611.
(26) Naito, A.; Ganapathy, S.; McDowell, C. A. *J. Am. Chem. Soc.* **1981**, *74*, 5393−5397.
(27) Naito, A.; Ganapathy, S.; McDowell, C. A. *J. Magn. Reson.* **1982**, *48*, 367−381.
(28) Gierasch, L. M.; Frey, M. H.; Hexem, J. G.; Opella, S. J. In *ACS Symposium Series No. 191: NMR Spectroscopy: New Methods and Applications*; Levy, G. C., Ed.; American Chemical Society: Washington, DC, 1981; Vol. 191, pp 223−247.
(29) Hexem, J. G.; Frey, M. H.; Opella, S. J. *J. Chem. Phys.* **1982**, *77*, 3847−3856.
(30) Diesveld, J. M.; Menger, E. M.; Edzes, H. T.; Veeman, W. S. *J. Am. Chem. Soc.* **1980**, *102*, 7935−7936.
(31) Grondona, P.; Olivieri, A. C. *Concepts Magn. Reson.* **1993**, *5*, 319−339.
(32) Eichele, K.; Wasylishen, R. E. *Solid State NMR* **1992**, *1*, 159−163.
(33) Gan, Z.; Grant, D. M. *J. Magn. Reson.* **1990**, *90*, 522−534.
(34) Menger, E. M.; Veeman, W. S. *J. Magn. Reson.* **1982**, *46*, 257−268.
(35) Harris, R. K.; Olivieri, A. C. *Prog. NMR Spectrosc.* **1992**, *24*, 435−456.
(36) Scheler, S.; Haubenreisser, H.; Rosenberger, H. *J. Magn. Reson.* **1981**, *44*, 134−144.
(37) Harris, R. K.; Jackson, P. J. *Phys. Chem. Solids* **1987**, *48*, 813−818.
(38) Naito, A.; Root, A.; McDowell, C. A. *J. Phys. Chem.* **1991**, *95*, 3578−3581.
(39) Sadiq, G. F.; Greenbaum, S. G.; Bray, P. J. *Org. Magn. Reson.* **1981**, *17*, 191−193.
(40) Stark, R. E.; Haberkorn, R. A.; Griffin, R. G. *J. Chem. Phys.* **1978**, *68*, 1996−1997.
(41) Bloom, M.; LeGros, M. A. *Can. J. Phys.* **1986**, *64*, 1522−1528.
(42) Tycko, R.; Opella, S. J. *J. Am. Chem. Soc.* **1986**, *108*, 3531−3532.
(43) Tycko, R.; Opella, S. J. *J. Chem. Phys.* **1987**, *86*, 1761−1774.

nitrogen in a single crystal or uniaxially oriented sample. This is in contrast to the ^{14}N fundamental NMR spectrum where each nitrogen contributes a doublet offset from the Larmor frequency by the second-order shift.

Previous studies of ^{1}H resonances perturbed by ^{14}N have been limited to a few examples where the resonances from hydrogens bonded to nitrogens are broadened compared to those bonded to carbons in combined multiple-pulse magic angle spinning (CRAMPS) experiments.[36-38] The results presented here demonstrate that heteronuclear correlation solid-state NMR spectroscopy can be used to separate and resolve asymmetric ^{1}H triplet resonances and correlate them with the ^{14}N resonances for the nitrogens to which the hydrogens are bonded. High-resolution one-dimensional ^{1}H NMR spectra of hydrogens directly bonded to nitrogens can be extracted from two-dimensional ^{14}N fundamental ($\Delta m = 1$) and ^{14}N overtone ($\Delta m = 2$) spectra. In the two-dimensional heteronuclear correlation experiments, ^{14}N magnetization is detected during t_2 in the presence of high-power ^{1}H irradiation for decoupling. The ^{1}H resonances are narrowed through the application of homonuclear multiple-pulse decoupling during t_1 and are characterized indirectly by their effect on the ^{14}N resonances. The $^{1}H/^{14}N$ heteronuclear correlation experiments yield spectral parameters that can be used to measure ^{1}H chemical shift, $^{1}H/^{14}N$ heteronuclear dipole–dipole couplings, ^{14}N second-order shift (twice the second-order quadrupole shift plus twice the ^{14}N chemical shift), and the first-order quadrupole splitting.

The asymmetric dipole–dipole triplets observed in ^{1}H NMR spectra provide substantially more structural information than do the corresponding symmetric doublets observed in the ^{14}N overtone, ^{14}N fundamental, or ^{15}N spectra from the hydrogen–nitrogen dipole–dipole interactions at the same sites. This approach is best suited for amide sites where the ^{14}N has a large quadrupole coupling constant and a single bonded hydrogen. The graphical restriction plot method[44-47] for determining molecular structures from solid-state NMR spectral parameters clearly demonstrates the advantages of using the splittings from asymmetric triplets over those from the symmetric doublets. This is illustrated by determining the peptide plane orientation in a single crystal of *N*-acetyl-D,L-valine (NAV) from these measurements.

Experimental Section

The experiments were performed on a single 30-mg crystal of *N*-acetyl-D,L-valine with all nuclei present in natural isotopic abundance. The material was purchased from Sigma Chemical Co. and the crystal grown by slow evaporation from an ethanol/water solution.

The experiments were performed on a home-built spectrometer with a 8.4 T magnet, having ^{1}H and ^{14}N overtone resonance frequencies of 360.3 and 52.0 MHz, respectively, and on a Chemagnetics CMX-400 spectrometer with a 9.3 T magnet, having ^{1}H and ^{14}N fundamental and ^{14}N overtone resonance frequencies of 400.0, 28.9, and 57.7 MHz, respectively. In both spectrometers the sample was placed at an arbitrary orientation in a horizontal solenoidal coil that could be tuned to all resonance frequencies without moving the sample in the course of obtaining the various sets of experimental data. All measurements were made at room temperature. The data were processed using the FELIX program (Biosym).

Results

$^{1}H/^{14}N$ Heteronuclear Correlation Spectroscopy. The pulse sequence diagramed in Figure 3 was used to obtain the experimental $^{1}H/^{14}N$ overtone heteronuclear correlation data presented in Figures 5–7. In this two-dimensional experiment, the ^{1}H magnetization evolves under the influence of ^{1}H chemical shift and $^{1}H/^{14}N$ heteronuclear dipole–dipole interactions during t_1 with $^{1}H/^{1}H$ homonuclear dipole–dipole interactions suppressed through application of the multiple-pulse sequence. Each t_1 time increment corresponds to an integral number of complete multiple-pulse cycles. The phase and frequency-switched flip–flop Lee–Goldburg pulse sequence (FFLG-2)[48-50] was utilized because it combines a high degree of line-narrowing with a reasonable scaling factor (0.58) for the $^{1}H/^{14}N$ splittings and the ^{1}H chemical shifts, and it has a short cycle time, which is essential because short t_1 increments are required to give an ω_1 spectral width after Fourier transformation adequate for detecting the outer lines of the asymmetric ^{1}H triplets resulting from the $^{1}H/^{14}N$ dipole–dipole interactions without aliasing. Variations of this approach are highly effective in $^{1}H/^{15}N$ heteronuclear spectroscopy as well.[4,7] When the pulse sequence in Figure 3 is used for $^{1}H/^{14}N$ overtone heteronuclear correlation spectroscopy it differs from sequences used for $^{1}H/^{13}C$,[51-53] $^{1}H/^{15}N$,[54] or $^{1}H/^{14}N$ fundamental heteronuclear correlation spectroscopy in that the $\pi/2$ pulse width of the ^{14}N overtone channel is substantially different from that of the ^{1}H channel; this is a consequence of the nutation frequency for ^{14}N overtone transitions typically being an order of magnitude smaller than that for ^{2}H (with a nearly identical resonance frequency) at equivalent rf power levels.[43] Because the nutation frequency depends on molecular orientation, the pulse width at the ^{14}N resonance frequency was chosen empirically to optimize the ^{14}N overtone signal intensities. Spin-diffusion does not interfere with the coherence transfer process because of the application of an additional fixed interval with multiple pulse decoupling, and only short delays were needed before and after the pulses used to transfer coherence in order to allow it to defocus and refocus. These delays were also optimized for maximum signal intensities. The ^{14}N overtone magnetization generated by coherence

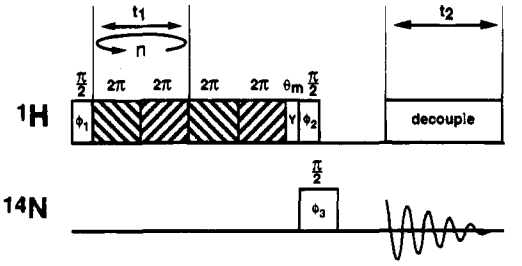

Figure 3. Schematic timing diagram of the pulse sequence used to obtain both ^{14}N fundamental and ^{14}N overtone two-dimensional $^{1}H/^{14}N$ heteronuclear correlation NMR spectra. The homonuclear multiple-pulse decoupling during t_1 is accomplished with the off-resonance frequency-switched Lee–Goldburg (FFLG-2) pulse sequence. Quadrature detection is accomplished in t_1 by collecting two free induction decays (FIDs), designated as "real" and "imag" in Table 1, for each t_1 increment with P_1, P_2, and acquisition phase cycling according to Table 2. The pulse width for the ^{14}N irradiation should correspond to $\pi/2$ nutation to induce maximum coherence transfer. In ^{14}N overtone spectroscopy, the pulse width is usually an order of magnitude longer than that for the ^{1}H channel.

(44) Stewart, P. L.; Valentine, K. G.; Opella, S. J. *J. Magn. Reson.* **1987**, *71*, 45–61.
(45) Opella, S. J.; Stewart, P. L.; Valentine, K. G. *Q. Rev. Biophys.* **1987**, *19*, 7–49.
(46) Opella, S. J.; Stewart, P. L. *Meth. Enzymol.* **1989**, *176*, 242–275.
(47) Chirlian, L. E.; Opella, S. J. *New Polym. Mater.* **1990**, *2*, 279–290.
(48) Lee, M.; Goldburg, W. I. *Phys. Rev.* **1965**, *140A*, 1261–1271.
(49) Mehring, M.; Waugh, J. S. *Phys. Rev. B.* **1972**, *5(9)*, 3459–3471.
(50) Bielecki, A.; Kolbert, A. C.; de Groot, H. J. M.; Griffin, R. G.; Levitt, M. H. *Adv. Magn. Res.* **1990**, *14*, 111–124.
(51) Caravatti, P.; Bodenhausen, G.; Ernst, R. R. *Chem. Phys. Lett.* **1982**, *89*, 363–367.
(52) Caravatti, P.; Bransehweiler, L.; Ernst, R. R. *Chem. Phys. Lett.* **1983**, *100*, 305–310.
(53) Roberts, J. E.; Vega, S.; Griffin, R. G. *J. Am. Chem. Soc.* **1984**, *106*, 2506–2512.
(54) Kumar, B. S. A.; Opella, S. J. *J. Magn. Reson.* **1991**, *95*, 417–420.

Table 1. Phase Cycling Scheme to Achieve Quadrature Detection in the Two-Dimensional Heterocorrelation Experiment

		ϕ_2		
cycle	ϕ_1	real	imag	ϕ_3
1	X	X	Y	X
2	$-X$	X	Y	$-X$
3	X	$-X$	$-Y$	$-X$
4	$-X$	$-X$	$-Y$	X

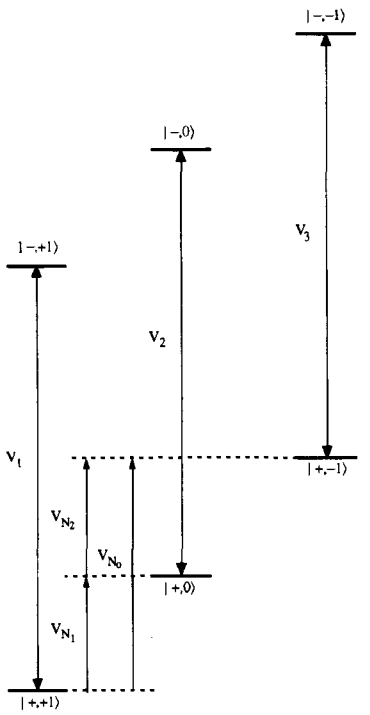

Figure 4. Energy level diagram for the isolated $^{14}N-^{1}H$ spin pair with each level labeling as $|\pm,+1\rangle$, $|\pm,0\rangle$, and $|\pm,-1\rangle$ corresponding to $m_I = \pm^1/_2$ and $m_S(N) = 1$, 0, and -1. The coherences connecting two energy levels which are $\Delta m = 1$ for ^1H are labeled as ν_1, ν_2, and ν_3. The ^{14}N coherences connecting two energy levels with $\Delta m = 1$ are labeled as ν_{N_1} and ν_{N_2} and the $\Delta m = 2$ are labeled as ν_{N_0} for the overtone.

transfer from the ^1H magnetization present at the end of the t_1 interval was detected under high-resolution conditions during t_2 with continuous ^1H irradiation.

Quadrature detection in the t_1 dimension was implemented with the hypercomplex method.[55] Two sets of data, corresponding to the real and imaginary parts of complex t_1 signals, were collected according to the phase cycling scheme in Table 1. After Fourier transformation and phase correction, the imaginary parts of both data sets were discarded and the real parts combined to form the complex data for the t_1 dimension, which were then processed using normal complex Fourier transformation.

Details of the coherence transfer process for $^1H/^{14}N$ spin pairs are illustrated in Figure 4. The three ^1H coherences resulting from a ^1H nucleus coupled to a ^{14}N nucleus are separated by only a few kilohertz and can be excited simultaneously. However, the ^{14}N coherences, ν_{N_1}, ν_{N_2}, and ν_{N_0}, must be excited and observed individually because they may be separated by as much as several megahertz, depending on the molecular orientation. The amplitude of the ^{14}N coherence transferred from ^1H depends on the population difference of the two energy levels generating the ^{14}N coherence at the end of the t_1 period, which in turn is modulated by the evolution during t_1 and the frequencies of coherences connecting other energy levels. For example, the amplitude of ν_{N_1} depends on the population difference of both $|+,+1\rangle$ and $|+,0\rangle$ states which in turn are modulated by the duration t_1 and, without considering energy level mixing, the frequency ν_1 connecting $|+,+1\rangle$ to $|-,+1\rangle$ and the frequency ν_2 connecting $|+,0\rangle$ to $|-,0\rangle$. Assuming no mixing of the energy levels, when one ^{14}N coherence is excited in the heteronuclear correlation experiment, only two lines of the asymmetric triplet can be transferred from ^1H to ^{14}N. However, the complete triplet pattern can be reconstructed from two separate heteronuclear correlation experiments exciting different ^{14}N coherences.

The effects of energy level mixing due to the ^{14}N quadrupole interaction cannot be ignored when the quadrupole coupling constant and Larmor frequency are similar in magnitude, as is the case for amide nitrogens in currently available magnets. The Hamiltonian operative during the evolution period will cause mixing with terms including S_z and can be described as $\langle\psi_m|S_z|\psi_n\rangle = mC_{nm} + C^*_{mn}$ where C_{mn} is a function of ν_Q/ν_{OS}.[43] The populations of all energy levels will also be a function of nearby coherences whose effects will be influenced by the mixing coefficient, which can be estimated from the experimental measurement of the nutation frequency to be in the range of 0.1 to 0.01. An effect of energy level mixing is that the entire asymmetric triplet is detectable even when only one ^{14}N coherence is excited, although the intensity of one line of the triplet will be much weaker than the other two.

Each NAV molecule contains one nitrogen; however, the crystal has two magnetically inequivalent molecules in the unit cell and the proton decoupled ^{14}N spectrum has four resonances in fundamental spectroscopy and two resonances in overtone spectroscopy.[56] The experimental ^{14}N fundamental two-dimensional heteronuclear correlation spectrum of a single crystal of NAV obtained with the pulse sequence in Figure 3 is presented in Figure 5 as a contour plot. Note the very large frequency scale (with breaks) in the ^{14}N fundamental frequency dimension. The spectrum in Figure 5 is a composite of the results from four separate experiments, each of which had the probe tuned and the carrier frequency set near one of the ^{14}N resonances. The ^1H carrier frequency was kept constant. An asymmetric ^1H triplet resonance can be reconstructed from these data by combining the ^1H doublets from the two ^{14}N resonances from the same molecule. The ^{14}N overtone two-dimensional heteronuclear correlation spectrum was also obtained on the same sample in the same orientation. Fundamental and overtone resonances were assigned to the respective molecules by comparing quadrupole splittings and second-order shifts. Spectral slices for one NAV molecule obtained from fundamental and overtone spectra are shown in Figure 6. The presence of the center resonance of the triplet in the overtone spectrum is confirmed by comparison with the fundamental spectra. As expected, the intensity of the central resonance is weaker than the two outer resonances. The asymmetry of the triplet for this particular orientation is small. Since the final ^{14}N coherence transferred from the protons, using two $\pi/2$ pulses, originates from antiphase components $\langle|^+S_z\rangle = \langle|_xS_z\rangle + \langle|_yS_z\rangle$ evolved during t_1, the spectrum along the ^1H dimension appears to be antiphase.

The experimental contour plot presented in Figure 7 is the result of a $^1H/^{14}N$ overtone heteronuclear correlation experiment performed on the same sample at a different orientation in the magnet. The two ^{14}N overtone resonances are resolved along

(55) States, D. J.; Haberkorn, R. A.; Ruben, D. J. *J. Magn. Reson.* **1982**, *48*, 286–292.

(56) Tycko, R.; Stewart, P. L.; Opella, S. J. *J. Am. Chem. Soc.* **1986**, *108*, 5419–5425.

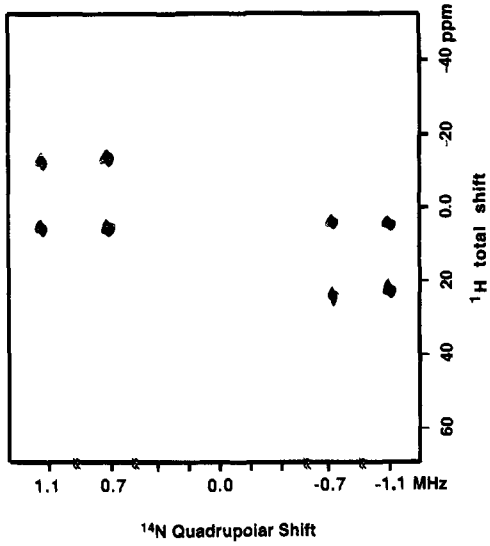

Figure 5. Composite experimental contour plot corresponding to a complete ^{14}N fundamental two-dimensional ^{1}H/^{14}N heteronuclear correlation spectrum. The contour plot results from the application of the pulse sequence outlined in Figure 3 to a single crystal of NAV and then adding all of the data together for plotting. The spectrum was obtained in four parts. The ^{14}N carrier frequency and probe tuning were optimized for each of the four ^{14}N fundamental resonances. The two signals at ±0.7 MHz are from one molecule and the pair at ±1.1 MHz are from the other molecule in the unit cell. The frequency shift along the ω_2 axis is relative to the ^{14}N Larmor frequency of 28.87 MHz in a 9.3-T field. The ^{1}H resonances along the ω_1 axis associated with each of the ^{14}N resonances consist of two lines from the ^{1}H asymmetric triplet. The frequency scale along the ω_1 axis is referred to as the ^{1}H total shift, since the observed resonance frequencies result from the ^{1}H chemical shift and the ^{1}H/^{14}N heteronuclear dipole−dipole interactions. One part per million equals 400 Hz after correction for scaling by the pulse sequence. t_1 increments of 36.8 μs were used corresponding to a sweep width of 46.85 kHz after scaling. The $\pi/2$ pulse widths for ^{1}H and ^{14}N are 2.8 and 3.2 μs, respectively. Each spectrum resulted from signal averaging 128 transients for each of 32 t_1 points. The recycle delay was 5 s.

the ω_2 frequency axis of the two-dimensional spectrum with their resonance frequencies determined by the second-order ^{14}N quadrupole shift and ^{14}N chemical shift, both of which vary as a function of the orientation of the amide site in the magnetic field.

Each ^{14}N overtone resonance is correlated with an asymmetric ^{1}H triplet resonance along the ω_1 frequency axis in the two-dimensional spectrum in Figure 7. The frequencies of the ^{1}H resonances are a function of the ^{1}H/^{14}N heteronuclear dipole−dipole interaction, as influenced by both the ^{14}N quadrupole interaction and the ^{1}H chemical shift. Resolution of the components of the ^{1}H triplets is achieved because of the effectiveness of the homonuclear decoupling by the multiple-pulse sequence. It should be possible to obtain substantially narrower ^{1}H line widths through further optimization of the instrumentation and experimental conditions, which would make this experimental approach generally applicable for obtaining high-resolution spectra of single-crystal and oriented molecules.

In principle, effects of the heteronuclear dipole−dipole interaction can be observed in the spectra of both nuclei, depending on the choice of experiments. The one-dimensional ^{14}N overtone NMR spectrum obtained without ^{1}H decoupling has each resonance split into a symmetric doublet; however, it is generally more effective to observe ^{14}N resonances split into doublets by heteronuclear dipole−dipole interactions in two-dimensional separated local field spectra,[43,56] which can be obtained with and without multiple-pulse decoupling, providing

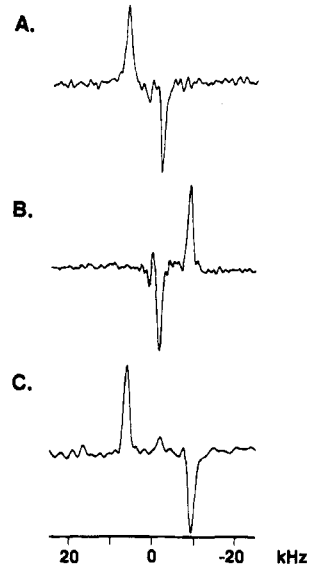

Figure 6. (A and B) ω_2 slices from the fundamental spectra in Figure 5 at −0.7 and +0.7 MHz, respectively. (C) A slice from the corresponding overtone spectrum obtained from the same sample without changing orientation. This comparison illustrates how the composite spectrum in Figure 5 can give the full ^{1}H NMR spectra associated with the ^{14}N fundamental resonances. It also demonstrates how the same interactions are manifested in fundamental and overtone ^{14}N NMR spectra.

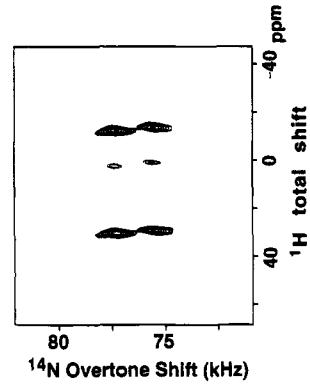

Figure 7. Contour plot of an experimental ^{14}N overtone two-dimensional ^{1}H/^{14}N heteronuclear correlation spectrum of a NAV at a different orientation than that used to obtain the data in Figures 5 and 6. The overtone shift is relative to twice the ^{14}N Larmor frequency in a 8.4-T field. The two ^{14}N overtone resonances result from the two magnetically distinct molecules in the unit cell. The ^{1}H resonances along the ω_1 axis associated with the ^{14}N overtone resonances are asymmetric triplets, as expected from the ^{1}H/^{14}N dipole−dipole interaction. The frequency scale along the ω_1 axis is referred to as the ^{1}H total shift, since the observed resonance frequencies result from the ^{1}H chemical shift and the ^{1}H/^{14}N heteronuclear dipole−dipole interactions. One part per million equals 360 Hz after correction for scaling by the pulse sequence. t_1 increments of 45.6 μs were collected resulting in a sweep width of 37.81 kHz, after scaling. The spectrum resulted from signal averaging 256 transients for each of 32 t_1 points. The recycle delay was 5 s.

a convenient way to measure the experimental scaling factor. Since the frequency splitting of the outer two lines of the triplet should be approximately equal to the splitting observed in the separated local field experiment obtained with multiple pulse decoupling, this gives an additional check on the experimental measurements.

The asymmetry of the triplets is clearly evident in the spectra obtained at this orientation of the crystals and the frequencies for each component of the ^{1}H resonance triplets can be measured directly. The ^{1}H resonance frequencies observed in the spectrum

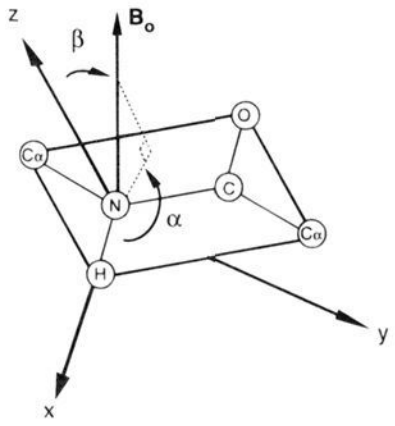

Figure 8. Molecular axis system for the peptide plane. The x axis is coincident with the NH bond, the z axis is perpendicular to the plane, and the y axis is orthogonal to x and z. The orientation of the peptide plane with respect to direction of the applied magnetic field, B_0, is described by α and β. β is the angle between the x axis and the projection of B_0 in the x, y plane.

in Figure 7 are listed in Table 1, taking into account the experimental scaling factor from the multiple-pulse cycle applied during t_1. The ^{1}H resonance frequencies reflect both the ^{1}H/^{14}N heteronuclear dipole−dipole and ^{1}H chemical shift interactions. The resolution is sufficient to resolve the ^{1}H chemical shifts within the approximately 15 ppm breadth of the ^{1}H amide chemical shift tensor.[4,57]

Structure Determination by Solid-State NMR Spectroscopy. Spectral parameters from all operative nuclear spin interactions vary with orientation in the magnetic field. This is the principle for the method for determining molecular structures of single crystal or uniaxially oriented samples by solid-state NMR spectroscopy.[45] Each spectral parameter has a characteristic dependence on the orientation of the bond or group with respect to the applied magnetic field, B_0, because of the anisotropy of the underlying nuclear spin-interaction. The angular dependencies for the various spectral parameters measurable in ^{14}N NMR spectra have been described[44] as have those for the triplets of a spin one-half nucleus bonded to ^{14}N.[12] Although a single spectral parameter is generally not sufficient to uniquely determine a molecular orientation, combinations of measurements provide such significant restrictions on the possible orientations that the structures of peptides and proteins can be determined.

Since more than one orientation is consistent with each spectral measurement and uncertainties from experimental errors and the tensors describing the spin-interactions need to be taken into account, we have developed a general graphical method to evaluate all the orientations that are consistent with each spectral measurement.[44−47] In this method the orientation of a peptide plane with respect to the direction of the applied magnetic field is characterized by the two angles, α and β, defined in Figure 8. The orientational dependence of the spectral parameters from all the spin interactions present in the nuclei in the peptide plane can be described as a function of these two angles. Although resonance frequencies, dipolar splittings, and other spectral parameters can be readily calculated from a single pair of α and β angles and the established magnitudes and directions of the principal elements of the relevant spin interaction tensors, an experimentally observed spectral parameter does not yield a single value for α and β, but rather a range of values for the pair of angles. This range reflects experimental errors, the uncertainty in the magnitudes and orientations of the principal elements of the spin interaction tensor, and ambiguities arising from the symmetry properties of the tensors.

Each measured spectral parameter places limits on the possible combinations of the values for α and β. The darkened areas on a restriction plot are those combinations of the angles α and β consistent with a single measured spectral parameter and the stereochemical properties of the peptide plane. α and β must lie between 0−360° and 0−180°, respectively, in order to accommodate all possible plane orientations. The superposition or intersection of the plots from multiple spectral parameters yields the orientations of the peptide plane consistent with all of the measured spectral parameters. In practice, the goal is to obtain the minimum number of plane orientations, which are represented by dark spots associated with individual pairs of α and β, with the minimum number of experimental measurements. In the most favorable cases, only two orientations are consistent with the experimental measurements, corresponding to "up" and "down" orientations of the peptide plane with respect to B_0; these describe the same structure, inverted by 180°, and are a consequence of the fact that none of the measurements can distinguish between a magnetic field vector that is up or down. Thus the two orientations consistent with the experimental data are described by a pair of angles α, β and its supplement, α + 180° and 180° − β.

To make a comparison between restriction plots generated from the spectral parameters measured in symmetric doublets and asymmetric triplets, spectra were simulated for the three peptide plane orientations shown in Figure 9. The asymmetries of the triplets vary greatly in these spectra, which indicates the high sensitivity of this parameter to the peptide plane orientation relative to the direction of the applied magnetic field. Restriction plots derived from the symmetric doublets and asymmetric triplets in the spectra for these three peptides plane orientation are shown in Figure 9, part D−I. The arrows indicate the pair of angles α and β corresponding to the actual orientation used to calculate the respective spectra. In each case conservative estimates of the experimental errors as well as uncertainties in

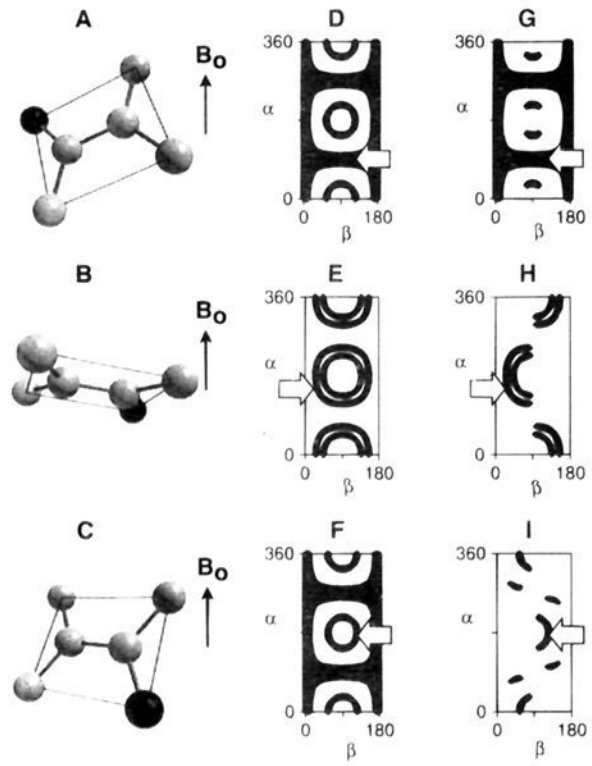

Figure 9. Illustration of how orientation influences the ^{1}H/^{14}N dipole−dipole interaction. (A) α = 90°, β = 125°. (B) α = 150°, β = 30°. (C) α = 175°, β = 125°. The calculated overtone dipolar couplings for A, B, and C are 13.8, 6.1, and 13.8 kHz, respectively. Restriction plots of orientation A, B, and C for overtone dipolar coupling are shown in parts D, E, and F. The calculated asymmetric triplets for A, B, and C are 6.9/0.0/−6.9, 2.7/0.6/−3.3, and −6.5/−0.8/7.3 kHz, respectively. Restriction plots of orientation A, B, and C for asymmetric triplets are shown in parts G, H, and I. The arrow in each restriction plot shows the orientation which the calculated results are based on. The comparison of restriction plots G−I and D−F clearly illustrates the advantage of observing the asymmetric ^{1}H triplets over the ^{14}N doublets, both of which result from the same dipole−dipole interaction.

(57) Gerald, R., II; Bernhard, T.; Haeberlen, U.; Rendell, J.; Opella, S. J. *J. Am. Chem. Soc.* **1993**, *115*, 777−782.

Table 2. ^{1}H and ^{14}N NMR Measurements for a Single Crystal of *N*-Acetyl-D,L-valine

parameter	molecule M1	molecule M2
^{14}N overtone shift (kHz)[a]	75.6 ± 0.5	77.3 ± 0.5
$^{14}N-^{1}H$ dipole–dipole splitting (kHz)[b]	13.5 ± 0.5	15.2 ± 0.5
^{1}H chemical shift (ppm)[c]	6.0 ± 0.5	7.3 ± 0.5
	8.5 ± 0.6	8.4 ± 0.6
$^{1}H-^{14}N$ dipole–dipole couplings	−1.5 ± 0.8	−1.5 ± 0.8
	−6.9 ± 0.6	−6.9 ± 0.6

[a] Referenced to twice the ^{14}N Larmor frequency (26.026 MHz). [b] Overtone. [c] Referenced to TMS at 0.0 ppm.

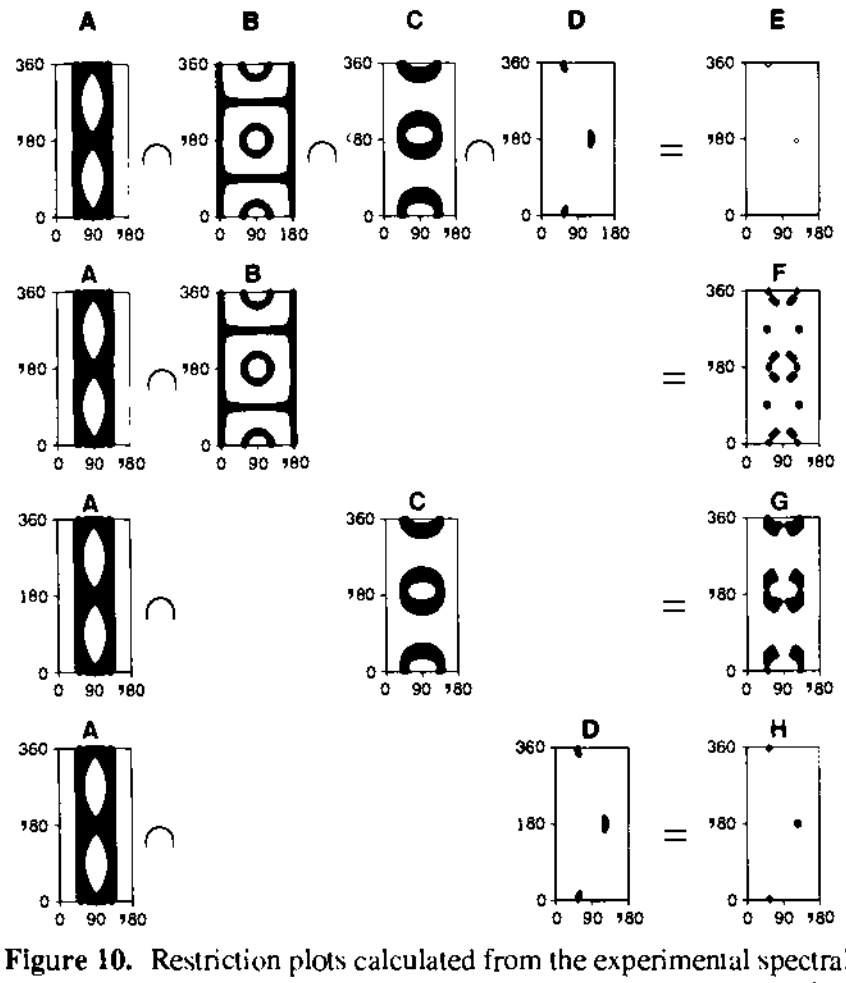

Figure 10. Restriction plots calculated from the experimental spectral data associated with one molecule in the unit cell of NAV: (A) ^{14}N overtone shift, (B) $^{14}N/^{1}H$ dipole–dipole splitting, (C) ^{1}H chemical shift, (D) $^{1}H/^{14}N$ dipole–dipole splittings, (E) the intersection of all four types of experimental data, (F) the intersection of the data obtained with a ^{14}N separated local field experiment alone, (G) the intersection of the data obtained with the ^{14}N overtone shift and ^{1}H chemical shift alone, and (H) the intersection of the data obtained with the ^{14}N overtone shift and $^{1}H/^{14}N$ dipolar splitting alone.

the molecular parameters governing the interaction are included in the orientation determination. Since both spectral parameters are from the same spin interaction, the restriction plots from the triplets are subsets of those from the doublets. These comparisons show that the asymmetry of the triplet discriminates among many possible orientations.

Values of four experimental spectral parameters from the NAV single crystal are listed in the Table 2. Restriction plots derived from the parameters from one of the molecules in the unit cell are presented in Figure 10. The superposition of plots from all four of the measured parameters yields two symmetry-related orientations for the peptide plane of the molecule designated M1, the minimum number of possible plane orientations, and the two plane orientations consistent with the experimental data in Figure 10 are shown in Figure 11. The symmetric dipolar coupling result can be excluded, since the restriction plot from an asymmetric triplet is a subset. As shown in this example, three restriction plots from two parameters that can be measured in one experiment are sufficient to determine the orientation of the peptide plane as long as one is an asymmetric triplet resulting from dipole–dipole coupling with a spin one nucleus.

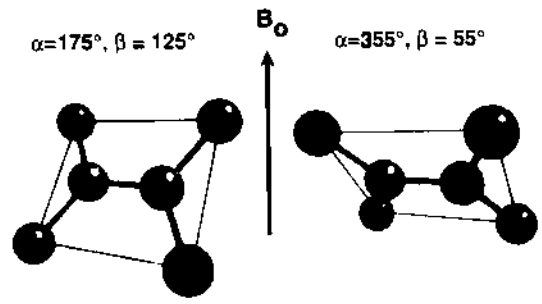

Figure 11. The two peptide plane orientation that corresponds to the intersections of restriction plots from all four spectral parameters listed in Table 1 for molecule M1 of the single crystal of *N*-acetyl-D,L-valine: (A) $\alpha = 175°$, $\beta = 125°$; (B) $\alpha = 355°$, $\beta = 55°$. The black spheres represent the amide hydrogen.

Discussion

The properties of the ^{1}H triplet, especially when compared to the ^{14}N doublet, provide dramatic illustrations of how dipole–dipole couplings are manifested in NMR spectra. In addition to the ^{1}H triplets, the $^{1}H/^{14}N$ heteronuclear correlation experiment enables the measurement of ^{1}H chemical shifts and correlates ^{1}H and ^{14}N resonances. This is advantageous because one experimental spectrum produces three spectral parameters that are highly orientationally dependent. Each triplet in the ^{1}H NMR spectrum provides much greater limitations on the orientations of the groups with respect to the direction of the magnetic field than the single splitting in the ^{14}N NMR spectrum for the same $^{1}H/^{14}N$ dipole–dipole interaction. The use of the triplet reduces the number of possible orientations consistent with the measurements, taking into account experimental error and uncertainty and bond lengths, to approximately half of those for the corresponding doublet for the same spin interactions. This reduction in orientations that are consistent with the spectral measurements is advantageous for determining the structures of peptides and proteins by solid-state NMR spectroscopy. Since dipole–dipole interactions are subject to motional averaging, these measurements have the potential to be used to describe molecular dynamics as well.

Acknowledgment. This research is supported by Grant Nos. R01GM29754 and R37GM24266 and postdoctoral fellowship F32GM13256 (to L.E.C.) from the General Medical Sciences Institute, National Institutes of Health and utilizes the Resource for Solid-State NMR of Proteins at the University of Pennsylvania, which is supported by Grant No. P41RR09731 from the Biomedical Research Technology Program, Division of Research Resources, National Institutes of Health.

JA950871M